Effect of heat exchange transient conditions with moving water-air interface on space charge accumulation in undersea HVDC cables

Giuseppe Rizzo
L.E.PR.E. HV Laboratory
University of Palermo
Palermo, Italy
giuseppe.rizzo07@unipa.it

Pietro Romano
L.E.PR.E. HV Laboratory
University of Palermo
Palermo, Italy
pietro.romano@unipa.it

Antonino Imburgia
L.E.PR.E. HV Laboratory
University of Palermo
Palermo, Italy
antonino.imburgia01@unipa.it

Fabio Viola
L.E.PR.E. HV Laboratory
University of Palermo
Palermo, Italy
fabio.viola@unipa.it

Giuseppe Schettino
L.E.PR.E. HV Laboratory
University of Palermo
Palermo, Italy
giuseppe.schettino@unipa.it

Graziella Giglia
L.E.PR.E. HV Laboratory
University of Palermo
Palermo, Italy
graziella.giglia@unipa.it

Guido Ala
L.E.PR.E. HV Laboratory
University of Palermo
Palermo, Italy
guido.ala@unipa.it

***Abstract*— The accumulation of space charge inside the dielectric layer of an HVDC cable is one of the most important issue to be considered in the design stage and during the operating conditions. The separation of space charge is due to several factors including the dependence on temperature of the electrical conductivity of the insulation and the establishment of a thermal gradient under load conditions. This research is focused on the investigation of the effect of an axial heat transmission on the space charge and electric field distributions in an HVDC cable. In order to assess the impact of this phenomenon, a case study involving a cable immersed partly in water and partly in air has been simulated by means of a 2-D thermal and electrical model in time domain. The electric field calculation is based on the quasi-static Maxwell model and the current continuity equation. To simulate the effect of waves, a moving water-air interface is considered, with time varying sinusoidal law. The results show the establishment of an electrical field peak near the water-air interface due to an increased temperature drop over the insulation in this area. The approach and the findings described in this article attempt to improve the knowledge in the relationship between thermal and electrical phenomena in HVDC cables. Moreover, this article focuses on the advisability of appropriately considering the impact of the axial heat transfer in the standards on the thermal rating of HVDC cables.**

Keywords*— *HVDC, cables, space charge, thermal rating, PEA, sustainable islands

I. Introduction

To date, particularly in the case of power transmission over long distances, HVDC extruded cables are among the most widely used technological solution. This is due to several reasons such as the lower costs, the better social acceptability and the performances respect to other solutions. On the other hand, it has been demonstrated that, unlike in HVAC, the electrical stress at which the insulation of an HVDC cable has to withstand does not depends only on the voltage [1]. During the normal operating conditions, the temperature drop over the dielectric thickness in HVDC cables leads to the accumulation of space charge until the spatial slope of the radial component of the electric field is reversed. This phenomenon is essentially due to the variability of the electrical conductivity of the insulation with exponential law with respect to temperature [2]. Beside the consequences of the onset of a thermal gradient, other phenomena concur to the accumulation of space charge, such as the injection from the electrodes, the trapping and de-trapping of electrons and ions [3-5]. However, it has been shown that, as the radial thermal gradient in the dielectric increases, the space charge density grows up until it leads to invert the radial slope' sign of the electric field distribution compared to that occurring under no load or alternating voltage. In this scenario, the maximum electric field value can be reached close to the outer surface of the dielectric layer and it may exceed that occurring under unloaded conditions [6]. The eventual achievement of electric field values higher than the rated ones can cause partial discharges [7-8] with consequent aging of the insulation and its breakdown [9]. The aging of the insulation layer can also be caused by thermal cycles that can degrade the crystalline lattice. This can lead to an appreciable modification of macroscopic physical properties, namely thermal and electrical conductivity. This can accentuate the above-mentioned phenomenon of reversal of the electric field profile [10]. The effects on HVDC cables of several transients, namely overvoltage and polarity reversal, are strictly related to the establishment of thermal gradient over the thickness of the insulation [11-12].

Hitherto, many researchers have focused their attention to the effect of the thermal gradient on the distribution of the electric field. Most part of these studies are based on a unidimensional characterization of the temperature distribution over the insulation layer obtained in accordance with the IEC 60287 standards [13-15]. In this case, the approach is based on a one-dimensional calculation of thermal resistances and, therefore, it does not take into account the axial thermal conduction. In addition, it should be noted that the current rating of HVDC cables at voltages higher than 5 kV is not covered by a dedicated IEC standard. The Cigrè brochure 640 pays attention to this lack and to the

need of considering the effect of the thermal drop over the insulation layer in the current rating of HVDC cables [16]. The same brochure emphasizes that the longitudinal heat flow through the cables can play an important role in the rating where axial discontinuity elements bring to a variation of the outgoing radial heat flux. In order to consider the axial heat transfer in joint bays, some researchers have proposed a 3D FEM model [17-19]. It has been shown that the weight of the space charge contribution in the insulation of HVDC cables due to the thermal gradient, compared to that due to other factors such as the injection of charge from the electrodes, increases with the cable diameter [20]. On the other hand, the thicker the insulation layer, the less effective the space charge measurement methods are. For this reason, at the state of the art, the assessment of these phenomena in large size HVDC cables by means of simulations can offer information that can be added to those obtainable from measurements on sample or less thick cables.

This research is part of a larger study on the distribution of the electric field within HVDC cables with varying thermal and electrical stress condition. In particular, the effect of the variation of the heat exchange conditions at the external boundary of the cable along its axial coordinate has been studied. In previous works, the authors have shown the effect of a not-moving water-air interface on an HVDC cable subjected to a constant load [21,22]. In this work, the consequences of a moving cable-water boundaries are considered in order to simulate the effect of the waves on a cable immersed partly in water and partly in air. In addition, the effect of a load increase with a step function in the middle of the simulated transitory has been evaluated.

In Fig. 1, a simplified schematic of the phenomenon deepen in this paper is shown. In a cable, the thermal conductivity of the conductor is up to three orders of magnitude higher than that of the insulation [14,23]. As will be discussed in the following sections, under certain conditions, this can lead the axial heat transfer through the conductor to prevail on the radial heat conduction through the dielectric layer. In presence of an abrupt variation in the heat exchange conditions at the boundary along the cable axis, the conductor in the cold section will be heated up by the conductor in the hot one by means of thermal conduction along the cable axis. On the contrary, the outermost part of the cable in the cold portion will reach almost the same temperature as the medium in which the cable is immersed. In other words, the heat can be mainly transmitted axially through the conductor and not through the insulation. This leads the temperature difference between the inner and outer surfaces of the dielectric layer to reach a peak value in the cold part just below the interface between the two mediums in which the cable is immersed.

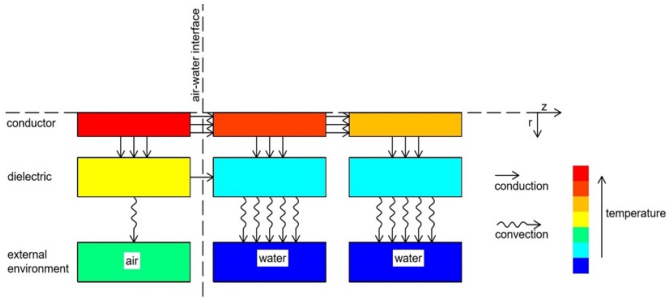

Figure 1. Simplified scheme of the phenomenon

As shown in section III, in a typical large size HVDC cable, the radial thermal resistance of the insulation is equal to the axial one of the conductor, for segments of about 0.5 m. Therefore, the above phenomenon can occur even if the interface position changes over time up to cover a range of about 1-2 m length. In this paper, a displacement of the interface within a range of 0.6 m has been considered. The above-described scenario can occur, for example, when an undersea HVDC cable emerges from the water. In this case, the outer surface of the cable is subjected to a strong variation of the external temperature and of the convective heat exchange coefficients in the axial direction. A sharp change along the axis of external thermal conditions could also occur in other scenarios, such as the crossing of another power cable, the proximity to heat sources or the presence of cold streams.

In order to study the above-described phenomenon considering the axial heat transfer and its effects on the space charge and electric field distributions, a 2-D axial symmetric numerical model has been implemented in Matlab®. The model used for this work is described in the second section, whilst, in the third section, a parametric study is offered to extend the results obtained for the specified case study to other cases. In the fourth section, the results of the simulation are presented. The findings of this study are discussed in the fifth section and the conclusions are presented in the sixth one.

II. 2-D COUPLED ELECTRO-THERMAL NUMERICAL MODEL

The 2-D axial symmetric adopted coupled electro-thermal numerical model is based on the hypothesis that the temperature, the radial component of the electric field and the electric current can vary only with the radius and the axial coordinate. The typical stratigraphy of an undersea HVDC cable is reproduced in accordance with the geometry shown in Fig. 2. With reference to the same figure, the conductor and the wire screen have been modeled as equivalent homogeneous materials considering a filling factor. For each layer, the properties of the material are defined in accordance with the table of material properties of IEC 60287-2-1 and IEC 853-2 standards. In particular, density, specific heat and thermal conductivity are used in the thermal model as well as permittivity and electrical resistivity at 20 °C define the material in the electric model. The electrical resistivity of the conductive material is calculated as a function of the temperature in order to upgrade, at each time step, the thermal power generation by Joule effect. On the contrary, an exponential relation is used for the estimation of the electrical conductivity of the dielectric depending on the temperature and the electric field [1]:

$$\sigma(T,E) = \sigma_0 \exp\left[a(T-T_0) + b(E-E_0)\right] \qquad (1)$$

where $\sigma(T,E)$ is the electrical conductivity of the dielectric at the temperature T and under the electrical field E, σ_0 is the electrical conductivity at the temperature T_0 equal to 20°C and under the electrical field E_0 equal to 0 V/m. The coefficients a and b are respectively the thermal and electrical dependence coefficients for the conductivity. As reported in literature, the value of b can be expressed as a function of the temperature. The values indicated in the reference [1] have been fitted with the following equation:

$$b = c(T-T_0)^2 + d(T-T_0) + e \qquad (2)$$

where c, d and e are the obtained constants depending on the material.

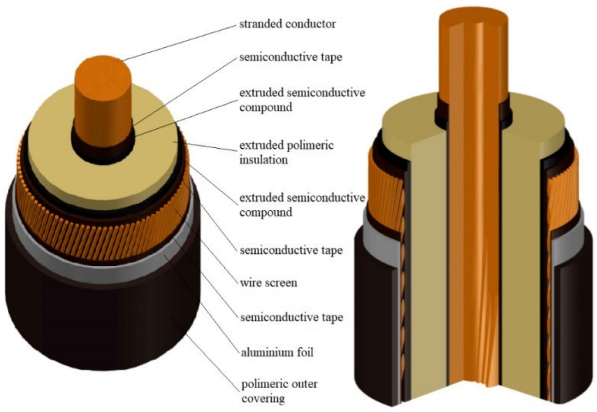

Figure 2. Typical HVDC cable

A time dependent current flows into the conductor producing a volumetric thermal power source depending also on its temperature dependent electric conductivity. The electric conduction through the insulation layer's thickness generates a thermal power density that is considered in the thermal model. This quantity is calculated at each time iteration of the model by considering the electrical conductivity defined by equation (1) and the radial current density J defined below. A convective heat exchange condition is applied to the outer surface. Furthermore, a time dependent DC voltage is applied between the conductor and the screen covering the outer semiconductive layer. In this case study, the voltage is considered constant whilst the current is kept constant until the middle of the simulated time range after which it passes to a higher constant value through a step function. For a given cable, the input data of the model are the applied voltage, the electric current, the convective heat transfer coefficient and the external temperature.

The first step of the electrical section of the model is to consider a guess distribution of radial electric field satisfying the following equations:

$$E(r,z,t) = -\nabla V(r,z,t) \quad (3)$$

$$\nabla \cdot \left(\varepsilon_0 \varepsilon_r(r) E(r,z,t)\right) = \rho(r,z,t) \quad (4)$$

where V is the voltage over the insulation layer, E is the electric field, ρ is the space charge density, ε_0 and ε_r are the relative and void permittivities respectively, r is the radius, z is the axial coordinate and t is the time. At the beginning of the transient, ρ is equal to zero. The electric field profile at the first iteration is similar to that occurring under an AC voltage in analogous conditions. Then the radial current density J is calculated from the Ohm's law for the current density:

$$J(r,z,t) = \sigma(r,z,t) E(r,z,t) \quad (5)$$

where σ is calculated from the equation (1) considering the local temperature at the current time. Once known the current density field over the insulation layer, the space charge density can be calculated by applying the current continuity law:

$$\nabla \cdot J(r,z,t) = -\frac{\partial \rho(r,z,t)}{\partial t} \quad (6)$$

Finally, the electric field radial distribution can be updated by resolving the equations (3) and (4).

The time dependent temperature distribution is calculated from the discretization of transient conductive heat transfer law expressed in cylindrical coordinates:

$$\frac{1}{r}\frac{\partial}{\partial r} k(r) r \frac{\partial T(r,t)}{\partial r} + \frac{\partial^2 k(r) T(r,t)}{\partial z^2} + q'''(r,t) = rh(r) C(r) \frac{\partial T(r,t)}{\partial t} \quad (7)$$

where $k(r)$ is the thermal conductivity, $T(r,t)$ is the temperature, $q'''(r,t)$ is the thermal power density, $rh(r)$ is the mass density, $C(r)$ is the specific heat and t is time. The above differential equations have been discretized by means of the finite differences' method applied to a structured mesh grid. Because the axial symmetry of the model, a flux equal to zero is set at $r = 0$ and at the axial boundaries. The continuity of heat flux is set at the interfaces between different materials.

III. The Role of the Cable' Size

As mentioned above, this paper is focused on the evaluation of the electric field peak reachable near the interface between two mediums in which an HVDC cable could be immersed. As described above, this value depends on the geometry of the cable, the properties of the materials of which it is composed and the external mediums' properties. In order to describe this phenomenon from a more general point of view, for a certain cable, the ratio between the axial and the radial thermal resistances can be considered. The thermal conductivities of copper and aluminum used for the core are typically three orders of magnitude higher than those of the insulating material. In the case of a cable having a copper core and XLPE insulation, the thermal conductivities are 390 W/(m*K) and 0.287 W/(m*K) respectively [14,23]. Therefore, the axial thermal resistance can be approximated as which of the conductor R_A that can be calculated as follows:

$$R_A = \frac{4l}{k_{cond} d_{cond}^2 \pi f} \quad (8)$$

Where l is the length of the cable section, k_{cond} is the thermal conductivity of the conductor material, d_{cond} is the diameter of the conductor and f is its filling factor.

The radial thermal resistance R_R of the dielectric can be estimated as follows:

$$R_R = \frac{\ln\left(\frac{d_{ext}}{d_{cond}}\right)}{2\pi l k_{diel}} \quad (9)$$

Where d_{ext} is the outer diameter of the dielectric and k_{diel} is its thermal conductivity. By setting ($R_A = R_R$), it is possible to find a value of l such that the axial thermal resistance is equal to the radial one:

$$l_{eq} = \sqrt{\frac{m}{8}\frac{k_{cond}}{k_{diel}}} \quad (10)$$

Where:

$$m = \ln(y) d_{cond}^2 f \quad (11)$$

Where:

$$y = \frac{d_{ext}}{d_{cond}} \quad (12)$$

Where l_{eq} is the length of a cable' segment where the axial and the radial thermal resistances are equals. The values of m and l_{eq} grow up with the diameter of the conductor and with the ratio y as shown in Figs. 3 and 4. The aptitude of a cable to be subjected to local electric field peaks related to axial thermal conduction could be defined by the above parameter l_{eq} that only depends on the characteristics of the cable. In other words, the higher is the value of l_{eq}, the higher is the ratio between axial and radial thermal resistances. Therefore, in the case of abrupt variations in the heat exchange conditions with the axial coordinate, as l_{eq} grows, the peak in the temperature drop over the insulation thickness increases.

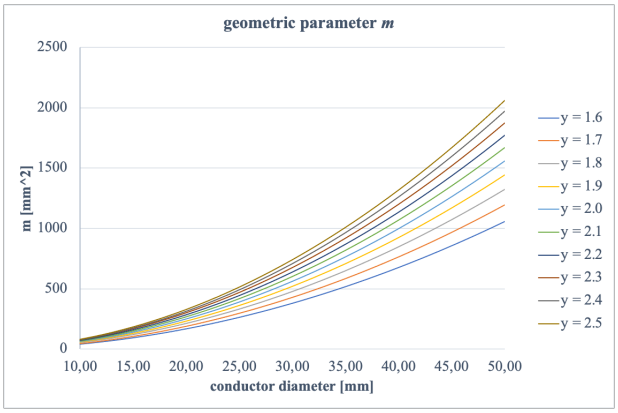

Figure 3. Geometric factor m vs conductor diameter at different values of ratio y and $f = 0.9$

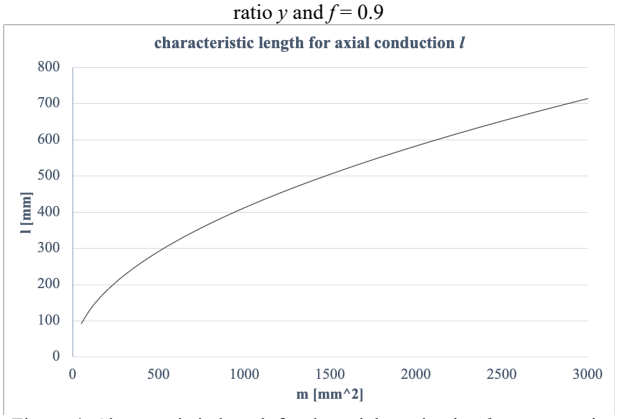

Figure 4. Characteristic length for the axial conduction l vs geometric parameter m

IV. Simulations and Results

As already underlined, a 2-D axial-symmetric numerical scheme in cylindrical coordinates, has been adopted. The effect of axially variable thermal boundary conditions has been investigated by considering a cross section of HVDC cable with a length of 10 m. At the cable's outer surface, a convective heat exchange has been considered, whilst, at the axial boundaries, an adiabatic condition has been applied. A sensibility analysis has demonstrated that the increase of the domain's axial length does not modify the results. Therefore, in order to optimize the calculation effort, the length of the modeled cable' segment has been limited to 10 m whilst the axial discretization has been optimized. The main geometric parameters and the boundary conditions used in the simulation, are listed in Table I. A copper conductor and a XLPE insulation material have been considered. A moving cable-water-air boundary is considered. In particular, the water and the air outside the cable, change over time with a sinusoidal law around the middle of the segment, with a period equal to 20 s and a peak-to-peak value equal to 0.6 m. This is accomplished by using the appropriate convective heat exchange condition on the external boundary of the cable. The duration of the transient is set equal to 48 h. An electric current equal to 1200 A flowing inside the conductor is set for the first 24 hours; then a current equal to 1920 A, corresponding to the rated value at 90 °C, is set for the second half of the transient. Typical values of convection coefficients for calm air and water are considered. The section immersed in water, which from now on called as "cold segment", is cooled by water at a temperature of 15 °C with a convective exchange coefficient of 100 W/(m^2*K).

TABLE I. Cables Properties and Boundary Conditions

Duration of the transient [h]	48
Conductor material	Copper
Insulation material	XLPE
Conductor radius [mm]	20
Cable external radius [mm]	63
Insulation thickness [mm]	30
Semiconductive layers thickness [mm]	1.0
Cable length [m]	10
Section immersed in air [m]	From 5 ± 0.3 to 10
Section immersed in water [m]	From 0 to 5 ± 0.3
Wave period of the moving interface [s]	20
Water temperature [°C]	15
Water convective heat exchange coefficient [W/(m^2*K)]	100
Air temperature [°C]	25
Air convective heat exchange coefficient [W/(m^2*K)]	8
Voltage [kV]	510
Current [A]	From 0 to 24 h: 1200 A From 24 to 48 h: 1920 A

The remaining cable portion, which from now on referred as "hot segment", is cooled by air with a temperature of 25 °C and the convective exchange coefficient is set to 8 W/(m^2*K). As shown in reference [24], a difference up to 10 K between the monthly averaged values of temperatures of sea surface and free air is consistent with conditions where the upwelling of cool water from the bottom into the sea surface occurs.

The voltage and the current are applied with a step function immediately when the simulation starts. In Fig. 5, the temperature drop over the insulation thickness at the end of the transient is shown, as a function of the axial coordinate. As it can be observed, the maximum temperature drop is reached in the cold segment just below the average level of the interface. The presence of the interface seems to influence a section of the cable with a length of approximately 6 m. With reference to previous articles of the authors, it can be stated that a moving sea level leads to increase the length of cable section subjected to the effect of the axial conduction and decrease the amplitude of the peak in the radial thermal gradient. In this case study, the entity of the radial thermal gradient reaches about a +14% with respect to the value in deep waters and +2.3% with respect to the value immersed in air. As can also be observed from the Fig. 5, due to the increase in the conductor electrical resistivity at high temperature, a higher thermal power generation in the cable core in the hot region leads the radial temperature drop to greater values in the hot region.

As shown in Fig. 6, during the load transient, the temperature drop over the radius never exceeds the maximum value achieved in steady state at rated conditions. On the other hand, as illustrated in the Fig. 7, the temperature drop is concentrated near the conductor during the first hours after the load increase. As shown in the Fig. 8, this leads the space charge density near the inner semiconductive layer to reach a peak during the first hours after the load abrupt increase. In this figure, the space charge distribution at the average interface level over time is shown. The results show that the highest concentrations of space charge lay in proximity of the

interfaces between the dielectric and the semiconductive layers. This is because the abrupt variation in permittivity. To emphasize the role of the space charge accumulation within the bulk of the dielectric, the peaks at the boundaries of the dielectric layer have been removed from the illustration. The space charge found is positive across the insulation thickness, therefore, the effect of the temperature dependency of the electric conductivity in dielectrics under HVDC voltage and load enhance the accumulation homocharges near the inner electrode and heterocharges in proximity of the outer one.

As it can be seen in Fig. 9, the aforementioned local and transient peak in space charge density close to the inner semiconductive layer does not cause an analogous behavior of the electric field distribution. At the beginning of the transient, the electric field vs radius profile assumes a hyperbolic-like pattern with maximum value in proximity of the inner surface. After approximately 4 h, this pattern has been definitively modified from the accumulation of space charge inside the dielectric and an equilibrium is reached with the maximum value reached near the outer surface. Immediately after the abrupt increase in load, the amount of space charge grows further leading the maximum electric field at the outer surface to overcome the initial maximum value reached at the inner boundary.

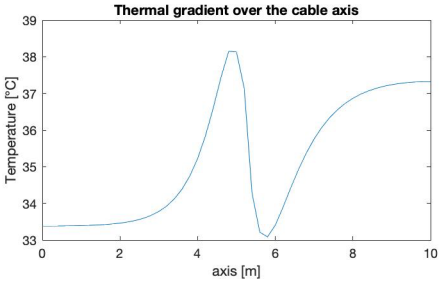

Figure 5. Temperature difference vs axial coordinate at the end of the transient t = 48 h

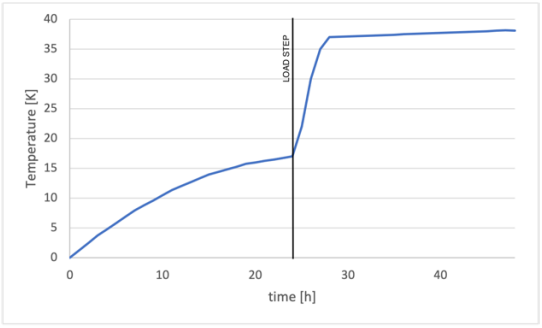

Figure 6. Temperature drop across the insulation at the water-air interface level over time

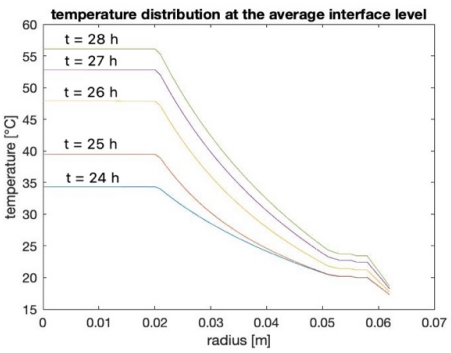

Figure 7. Radial temperature distribution at the average interface level after the load increase from t = 24 h

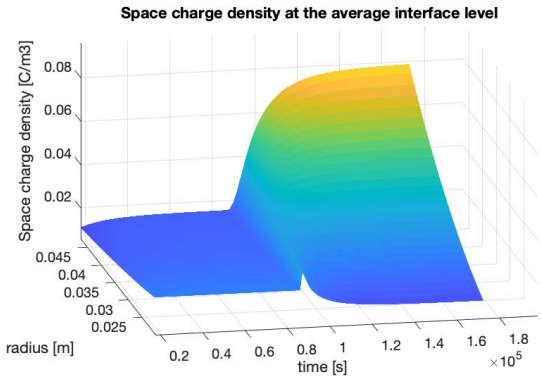

Figure 8. Radial space charge distribution at the average interface level vs time

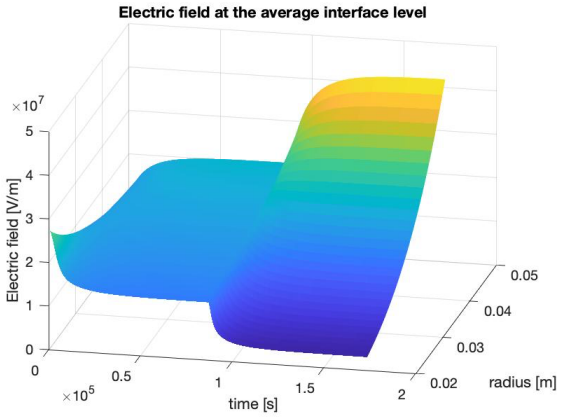

Figure 9. Electric field distribution at the average interface level vs time

In Figs. 10-12, the radial electric field distributions at different time steps and in different axial positions are shown. At the end of the simulated transient, the maximum electric field is reached on the outer surface of the dielectric layer for all the cross sections. As found in the authors' previous works in the case of a fixed interface between the fluids outside the cable, the maximum electric field value is reached just below the air-water average interface level [21-22].

For the simulated case study, this value is equal to 42.3 kV/mm and exceeds of 3 % the maximum electric field in the sections immersed in air, where the peak is equal to 41.1 kV/m. In the part of the cable immersed in water, at 5 m from the average interface level, the maximum electric field value is equal to 37.7 kV/mm.

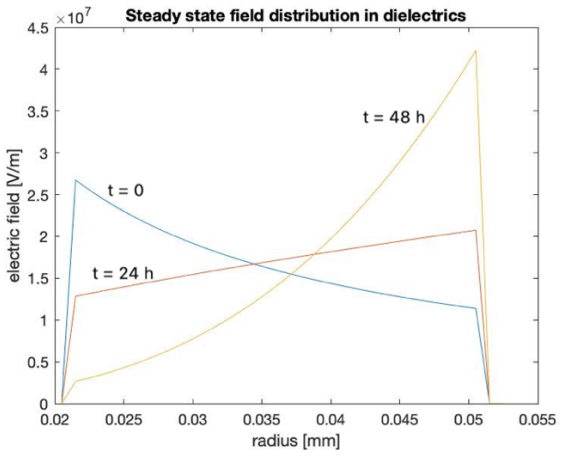

Figure 10. Inversion of the slope of the electric field profile – just below the interface

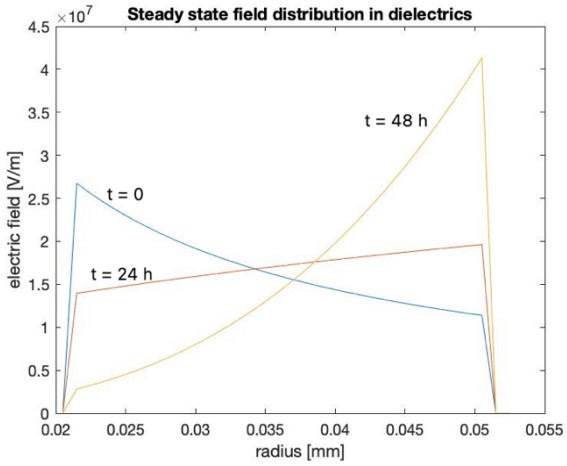

Figure 11. Inversion of the electric field profile – section immersed in air

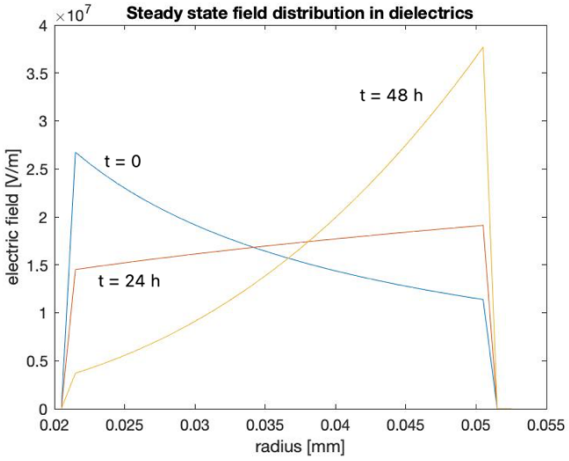

Figure 12. Inversion of the electric field profile – section immersed in water

In Figs. 13 and 14, the two profiles show the space charge spatial distribution in the middle and at the end of the transient, respectively. As mentioned above, at low loads, the space charge accumulation is dominated by the temperature drop. As it can be seen from the Figs. 13 and 14, the effect of the axial thermal conduction is more evident at the end of the transient than after the first 24 hours. Once reached the first steady state after 24 h from the beginning, the peak in space charge density is reached just below the average interface level and exceed its maximum value in the air-immersed region by 2.3 %. This percentage reaches the value of 5.6 % at the end of the transient. In Figs. 15 and 16, the two profiles illustrate the electric field distribution over the radial and axial coordinates of the cable. The electric field depends on the applied voltage and it is influenced by the space charge accumulation. As it can be observed in the figures, as well as the space charge density, the maximum values of the electric field are reached just below the average interface level.

V. Discussion

The results of this research show the effect, on the distributions of space charge and electric field inside the insulating layer of an HVDC cable, of the axial variation of the heat transfer conditions with the outside. The analysis has been carried out by means of simulations performed considering two different load levels. Furthermore, attention has been paid to the space charge and electric field trends during the transition between the two different phases.

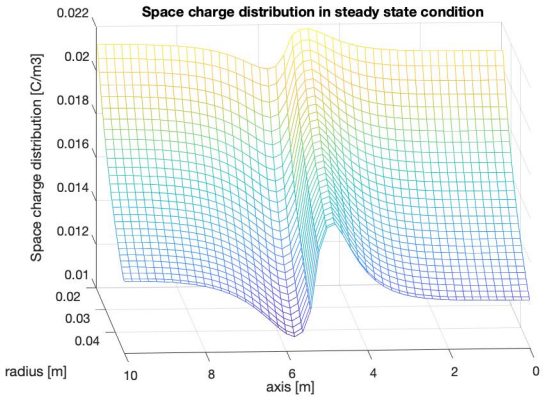

Figure 13. Space charge spatial distribution - t = 24 h

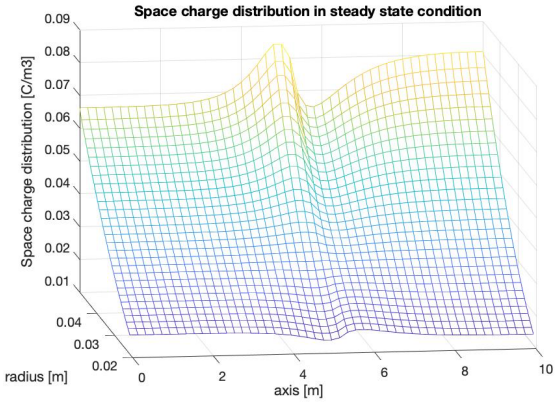

Figure 14. Space charge spatial distribution - t = 48 h

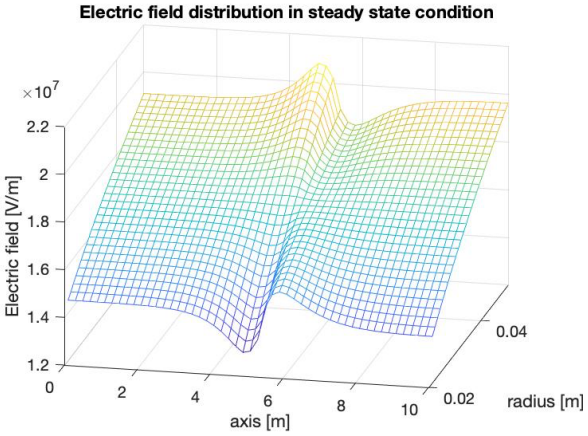

Figure 15. Electric field spatial distribution - t = 24 h

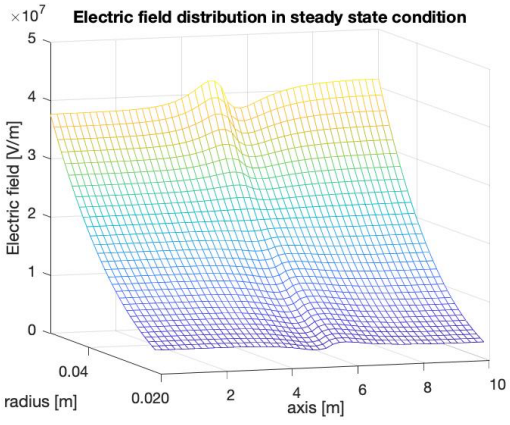

Figure 16. Electric field spatial distribution - t = 48 h

As it can be noticed from the Fig. 8, the growth in load causes the inversion of slope of the space charge profile because of the increased electrical conductivity of the dielectric at higher temperatures. This behavior can be explained considering the distribution of space charge density within the dielectric layer once reached the steady state. Assuming that the electric field varies only with the radius, this expression can be written as follows: [1]:

$$\sigma E \frac{d}{dr}\left(\frac{\varepsilon}{\sigma}\right) = \rho \tag{13}$$

Where ε is the permittivity of the insulation. In order to assess the radial slope of the space charge density, the (13) is derived as follows:

$$\frac{d\rho}{dr} = \frac{d}{dr}(\sigma E) \cdot \frac{d}{dr}\left(\frac{\varepsilon}{\sigma}\right) + \sigma E \frac{d^2}{dr^2}\left(\frac{\varepsilon}{\sigma}\right) \tag{14}$$

It is possible to demonstrate that the first term of the right-hand side part of the equation (14) is negative for the insulation layers subjected to HVDC voltage and under load. On the contrary, it can be proved that the second term assumes positive values due to the exponential trend of the electrical conductivity with the temperature and therefore with the radius. In the Fig. 17, the sign of the aforementioned derived terms, at the end of the simulated transient, are shown. Since σE is proportional with the temperature, the radial derivative of the space charge density passes from negative to positive values once exceeded a certain temperature. On the basis of the aforementioned reasons, it can be stated that the space charge profile depends on both the temperature drop and its average value. The former term prevails at low loads whilst the latter dominates when the current tends to its rated value. In other words, the higher the load, the higher the space charge accumulated near the cooler interface with the outer semiconductive layer.

After the first 24 h from the beginning, the peak in the electric field overcomes by 6.3% its maximum value in the air-immersed region. This percentage reaches the value of 3.0% at the end of the transient. It can therefore be stated that the effect of the axial thermal conduction on electric field peaks decreases as the load grows up. However, the increase in electric field due to the effect of the axial thermal conduction can be lower or higher depending on the type of cable and the boundary conditions. For example, in the event of a greater temperature difference between water and air or in the case of a less-moving water level, the increase in the electric field compared to that reached in the air section can be higher. The radial profile of the electric field established in a loaded cable could be seen as the sum of two contributions. At the electrostatic field distribution obtainable under equivalent alternating voltage, should be summed the "residual field" related to the accumulation of space charge. The latter can be considered as the electric field remaining at the instant immediately after a grounding event. As a consequence of the equations (3) and (4), this "residual field" assumes negative values in proximity of the inner surface of the dielectric layer and positive ones at the outer boundary. This can lead to a greater risk of failure during reverse polarity events. This risk can be amplified from the effect of the axial thermal conduction that increase the maximum absolute values of the residual electric field reached at the boundaries of the dielectric.

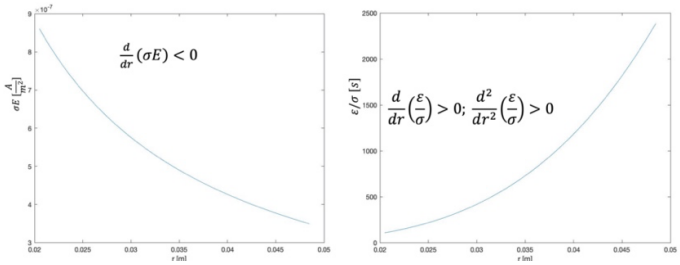

Fig. 17. Radial trends of the terms derived in the equation (14) at the end of the simulated transient

The model used in this research assumes that the separation of space charge inside a dielectric layer is exclusively due to the variation of electrical conductivity with temperature and electric field. Other phenomena contribute to the accumulation of space charge within the insulation layer of an HVDC cable and this can lead to quantitatively different results from those obtained in this research. These phenomena can be partly considered through bipolar charge transport models [25]. However, this approach requires a higher calculation effort compared to that needed from the model described in this paper. The latter has the main intent of obtaining a suitable thermo-electrical model for portions of cable several meters long.

VI. Conclusions

In this paper, the effect of axial variable external thermal conditions on HVDC cables is investigated. The study has been carried out by means of numerical simulations performed by means of a coupled electro-thermal model in time domain. A segment of a cable has been considered immersed half in water and half in air in order to evaluate the effect of the axially varying external heat exchange conditions on the radial thermal gradient. A moving water level and a load transient have been simulated to investigate the time trend of the electric field profile under different loads and dynamic conditions. By a comparison with previous works of the authors, where a fixed water lever was considered, it can be concluded that the thermal axial conduction leads to lower peaks in the electric stress in the case of moving interface. The maximum electric field is reached near the outer surface of the dielectric layer, just below the average interface level. This peak overcomes the maximum electric field achieved in the air-immersed region by 6.3% after 24 h from the beginning of the simulated transient. Once increased the load, this percentage decreases until it reaches the value of 3% at the end of the transient, when a new steady state condition has been achieved. This demonstrates that the increase in electric field due to the axial thermal conduction is smaller as the load increases, when other phenomena prevail. In fact, once a certain average temperature inside the insulation is exceeded, the slope of the radial space charge density profile changes sign. In the region immersed in air, on average warmer than that immersed in water, a greater space charge density towards the outside of the insulating layer leads to a considerable increase in the electric field in this area.

The results offered in this paper are indicatives and referred to a specific case study. As shown by Pilgrim et al., analogous phenomena can be observed in other conditions in which the heat exchange in HVDC cables and accessories cannot be modeled as one-dimensional. This article attempts to offer a contribute to generally define the aptitude of a cable to be subjected to local peaks in electric stress due to the axial

thermal conduction. With this purpose, a parameter depending only on the cable's geometry and materials has been defined. Other research in this direction can be carried out for the evaluation of the electric field distribution near joints, hot points along the cable length or proximity with other cables.

Based on the results of this research, it is desirable to introduce new standards for the thermal rating of HVDC cables considering the possible axial variation of heat exchange conditions with the outside and the evolution of the electric field profiles under dynamic conditions.

REFERENCES

[1] G. Mazzanti, M. Marzinotto; "Extruded Cables for High-Voltage Direct-Current Transmission - Advances in Research and Development"; IEEE press series on Power Engineering, 2013.

[2] T. T. N. Vu et al., "Electric field profile measurement and modeling in multi-dielectrics for HVDC application," 2013 IEEE International Conference on Solid Dielectrics (ICSD), Bologna, 2013, pp. 413-416.

[3] A. Imburgia, P. Romano, E. R. Sanseverino, F. Viola, N. Hozumi and S. Morita, "Space charge behavior of different insulating materials employed in AC and DC cable systems," 2017 International Symposium on Electrical Insulating Materials (ISEIM), Toyohashi, 2017, pp. 629-632.

[4] P. Romano, A. Imburgia and R. Candela, "Space Charge Measurement Under DC and DC Periodic Waveform," 2018 IEEE Conference on Electrical Insulation and Dielectric Phenomena (CEIDP), Cancun, 2018, pp. 293-296.

[5] M. De Araujo Andrade et al., "Different Space Charge Behavior of Materials Used in AC and DC Systems," 2017 IEEE Conference on Electrical Insulation and Dielectric Phenomenon (CEIDP), Fort Worth, TX, 2017, pp. 114-117.

[6] T. T. N. Vu, G. Teyssedre, B. Vissouvanadin, S. L. Roy and C. Laurent, "Correlating conductivity and space charge measurements in multi-dielectrics under various electrical and thermal stresses," in IEEE Transactions on Dielectrics and Electrical Insulation, vol. 22, no. 1, pp. 117-127, Feb. 2015.

[7] A. Imburgia, P. Romano, F. Viola, A. Madonia, R. Candela and I. Troia, "Space charges and partial discharges simultaneous measurements under DC stress," 2016 IEEE Conference on Electrical Insulation and Dielectric Phenomena (CEIDP), Toronto, ON, 2016, pp. 514-517.

[8] P. Romano, A. Imburgia, G. Ala, "Partial discharge detection using a spherical electromagnetic sensor", Sensors, vol. 19, no. 5, 2019.

[9] G. C. Montanari, "Bringing an insulation to failure: the role of space charge," in IEEE Transactions on Dielectrics and Electrical Insulation, vol. 18, no. 2, pp. 339-364, April 2011.

[10] C. C. Zhang, Y. F. Li, M. Y. Hu, F. L. Ma, H. Zhao and B. Z. Han, "Conductivity properties of XLPE insulation used for HVDC cable after accelerated thermal ageing," 2018 12th International Conference on the Properties and Applications of Dielectric Materials (ICPADM), Xi'an, 2018, pp. 500-503.

[11] Nugroho Adi et al., "DC Model Cable under Polarity Inversion and Thermal Gradient: Build-Up of Design-Related Space Charge"; Technologies 2017, 5, 46.

[12] N. Adi, G. Teyssedre, T.T.N. Vu, N.I. Sinisuka, "DC Field Distribution in XLPE-Insulated DC Model Cable with Polarity Inversion and Thermal Gradient", Proceedings of the 2016 IEEE International Conference on High Voltage Engineering and Application (ICHVE), Chengdu, China, 19–22 September 2016.

[13] IEC standard 60287-1-1 (2006), "Electric cables - Calculation of the current rating - Part 1-1: Current rating equations (100 % load factor) and calculation of losses – General".

[14] IEC standard 60287-2-1 (2015), "Electric Cables – Calculation of the current rating – Part 2: Thermal resistance – Section 1: Calculation of thermal resistance".

[15] IEC 60853-2:1989/AMD1:2008 "Amendment 1 - Calculation of the cyclic and emergency current rating of cables - Part 2: Cyclic rating of cables greater than 18/30 (36) kV and emergency ratings for cables of all voltages"

[16] CIGRE (2015), Technical Brochure 640, "A GUIDE FOR RATING CALCULATIONS OF INSULATED CABLES", WG B1.35.

[17] Pilgrim, J.A. Swaffield, D., Lewin, P. and Payne, D., (2008), "An investigation of thermal ratings for high voltage cable joints through the use of 2D and 3D finite element analysis," Conference record of the 2008 IEEE international symposium on electrical insulation, pp. 543-546.

[18] Pilgrim, J.A. Swaffield, D., Lewin, P., Larsen, S. and Payne, D., (2009), "Assessment of the impact of joint bays on the ampacity of high-voltage cable circuits," IEEE Transactions on power delivery, Vol. 24, No. 3, pp. 1029-1036.

[19] Huang, Z. Y., Pilgrim, J. A., Lewin, P. L.., Swingler, S. G. and Tzemis, G. (2014)., "Thermal-Electric Rating Method for Mass-Impregnated Paper-Insulated HVDC Cable Circuits", IEEE Transactions on Power Delivery, 30 (1), 437-444.

[20] D. Fabiani *et al*., "HVDC Cable Design and Space Charge Accumulation. Part 3: Effect of Temperature Gradient [Feature article]," in *IEEE Electrical Insulation Magazine*, vol. 24, no. 2, pp. 5-14, March-April 2008.

[21] G. Rizzo et al., "Space charge accumulation in undersea HVDC cables as function of heat exchange conditions at the boundaries – water-air interface," 2020 IEEE 20th Mediterranean Electrotechnical Conference (MELECON), Palermo, Italy, 2020, pp. 447-452.

[22] G. Rizzo, P. Romano, A. Imburgia, F. Viola, and G. Ala, "The Effect of the Axial Heat Transfer on Space Charge Accumulation Phenomena in HVDC Cables," Energies, vol. 13, no. 18, p. 4827, Sep. 2020.

[23] J. G. Hust and A.B. Lankford, "Thermal Conductivity of Aluminum, Copper, Iron, and Tungsten for Temperatures from 1K to the Melting Point," NBSIR-84/3007, pp. 1-16, 1984.

[24] H. Choi and Y. H. Zhang, "Monthly Variation of Sea-Air Temperature Differences in the Korean Coast," *Journal of Oceanography*, Vol. 61, pp. 359 to 367, 2005.

[25] E. Doedens, E. M. Jarvid, R. Guffond, and Y. V. Serdyuk, "Space Charge Accumulation at Material Interfaces in HVDC Cable Insulation Part II—Simulations of Charge Transport," Energies, vol. 13, no. 7, p. 1750, Apr. 2020.